Impact of the Refractive Index on the Achievable Rate of Liquid Crystal-Based Digital-RIS Indoor VLC Systems

Alain R. Ndjiongue, *Senior Member, IEEE*, Telex M. N. Ngatched, *Senior Member, IEEE*, and Octavia A. Dobre, *Fellow, IEEE*

***Abstract*—In wireless networks, reconfigurable intelligent surfaces (RISs) have recently been proven to have a significant impact. The RIS has been incorporated into wireless communication systems to improve security, increase coverage, reduce interference, and improve transmission quality. Digital RIS (DRISs) have also proven to provide better reflection management. However, the impact of the DRIS intrinsic parameters on the system's achievable rate, has not yet been investigated. Due to their availability and easily reconfigurable properties, liquid crystals (LCs) appear as suitable materials for use in DRIS, specifically in optical communication systems. This paper analyzes the effect of the LC's refractive index on the achievable rate of LC-based DRIS indoor visible light communication systems. Based on a set of discrete phase shifts, required refractive indices have been evaluated. The reflected power and achievable rates are determined with respect to incoming light wavelengths at 510 nm, 550 nm, and 670 nm. According to the obtained numerical results, there is no linear relationship between refractive indices, corresponding transition coefficients, phase shifts, light power, and achievable rate.**

***Index Terms*—Digital reconfigurable intelligent surfaces (DRISs), indoor visible light communication systems, liquid crystal-based DRIS, transmission rate, emerged light power.**

I. Introduction

THERE is an increasing interest in optical wireless communication (OWC) systems, including visible light communications (VLC) and free-space optical communications (FSO). These technologies are reported to be crucial components of beyond 5G and 6G networks [1], [2], [3]. This interest is primarily motivated by the advantages they offer as recently demonstrated in [3] and [4]. These advantages include cost-effectiveness, license-free frequencies, wider bandwidth, and higher channel capacities [3], [4]. Despite these advantages, the implementation of OWC technologies faces several challenges. For example, the directional nature of the FSO signal renders the FSO system vulnerable to obstruction from buildings, trees, or flying vehicles. On the other hand, indoor VLC can be affected by blockage of the line-of-sight (LoS) path by users [5]. A practical solution to this issue is the use of digital reconfigurable intelligent surfaces (DRISs), which also provide a partially reconfigurable channel.

The RIS is a newly introduced technology that is primarily used to improve signal coverage in wireless communication systems [3], [5]. In addition, the RIS technology provides wireless systems with a special advantage in terms of channel reconfiguration. It has also been used in radio frequency and VLC systems, to improve the quality of non-light-of-sight (NLoS) links, enhance coverage, reduce interference, and ensure security [2]. Recently, a digital version of the RIS, namely DRIS, has been proposed [6]. Its elements are fully digitized, with a code sequence made of k bits and composed of three main parts. The first part of the k bits activates the DRIS module, the second part controls the DRIS phase shift, while the third part represents the transition coefficient.

Among the plethora of materials available to be used in DRIS, liquid crystals (LCs) present the advantage of providing digital and smooth control of their intrinsic parameters. LCs are anisotropic materials, characterized by a refractive index, n, which is a combination of the ordinary and extraordinary refractive indices, n_o and n_e, respectively. LCs are also characterized by their optic axis, which is the direction in which a ray of transmitted light does not suffer birefringence. Birefringence is the double refraction experienced by light rays while crossing the LC's structure. All rays that are parallel to that direction are not affected by the LC's double refraction. As a result of the LC's anisotropic property, a light ray that passes through an uni-axial LC is generally split into two rays: the ordinary ray, which passes the crystal without any deviation, and the extraordinary ray which is deviated at the air-crystal interface. The two emerging rays, ordinary and extraordinary, have orthogonal polarization states. The LC's substance impacts incoming light rays on two main factors: the direction and intensity, which can be fully controlled by its refractive index, n. Thus, n has a noticeable impact on the system's achievable rate. For a noise power spectral density (PSD) in the range of 10^{-5} to 10^{-4}, up to 217.50 kbps of transmission rate variation can be observed. The specific objective of this paper is to investigate the influence of LC's intrinsic parameters, such as the refractive index, on

Manuscript received 7 October 2022; revised 29 November 2022; accepted 17 December 2022. Date of publication 20 December 2022; date of current version 28 December 2022. This work was supported in part by the Natural Sciences and Engineering Research Council of Canada (NSERC) through its Discovery Program. *(Corresponding author: Alain R. Ndjiongue.)*

The authors are with the Faculty of Engineering and Applied Science, Memorial University of Newfoundland, St. John's, NL A1C 5S7, Canada (e-mail: arndjiongue@mun.ca; tngatched@grenfell.mun.ca; odobre@mun.ca).

Digital Object Identifier 10.1109/JPHOT.2022.3230749

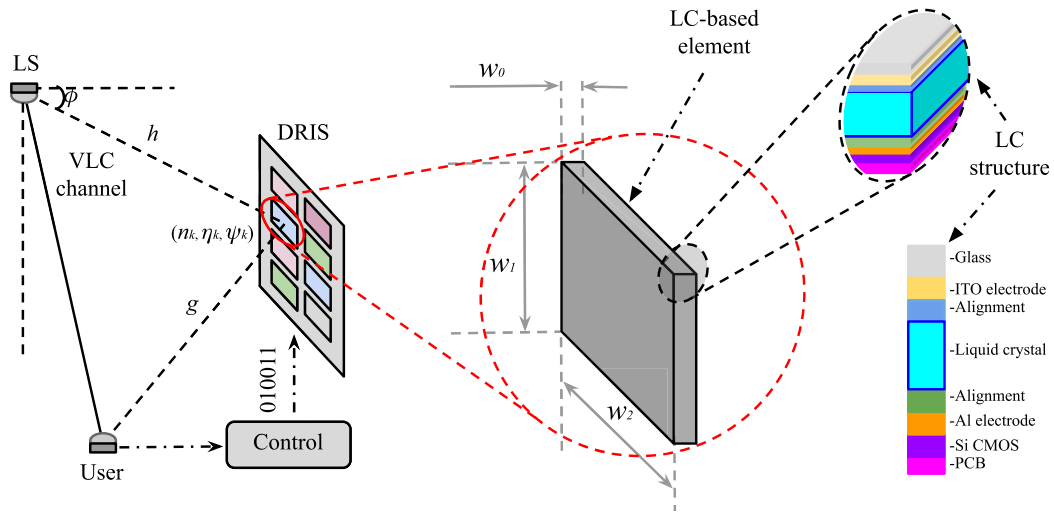

Fig. 1. LC-based DRIS-assisted VLC systems.

LC-based DRIS-assisted VLC systems' achievable rate. The contributions can be summarized as follows:

- An indoor VLC system assisted by DRIS is proposed and its achievable transmission rate is analyzed. Relationships between the LC's tilt angle and refractive index, and between phase shift and the externally applied voltage are discussed.
- Considering a set of impinging light wavelengths, the emerged light power and achievable transmission rate are evaluated, and numerical results are presented.

To the best of the authors' knowledge, such an analysis has not been previously published in the open literature. The remainder of this paper is organized as follows. The system and channel models, and the control process of DRIS elements are presented and discussed in Section II, while the achievable transmission rate is derived in Section III. Numerical results are provided in Section IV. Finally, the implementation complexity is discussed and conclusions are drawn in Section V.

II. System Model, DRIS Elements, and Control Operation

A. System and Channel Models

Fig. 1 depicts a DRIS-based VLC system, where the LoS link from the light source can be randomly disrupted. In this situation, a non-LoS (NLoS) path can be provided by a deployed DRIS. The DRIS, made of LC-based elements, reflects the light toward the users. The DRIS element's structure, depicted on the right hand side of Fig. 1, reveals a number of parallel transparent plates. The top layer is a glass substrate with an anti-reflective characteristic, followed by an Indium tin oxide (ITO) electrode to connect the externally applied electric field, in conjunction with the aluminum (Al) electrode on the other side of the LC substance. Two alignment layers sandwich the LC layer, and a Silicon (Si)-complementary metal-oxide-semiconductor (CMOS) layer is used to control the cell's temperature while acting as a perfect mirror. The structure sits on a printed circuit board (PCB). The LC layer, which constitutes the core of the DRIS element, depends on its substance and dye, and is characterized by its phase shift and transition coefficient. In this paper, we assume that, except the LC layer, no other plate induces a phase shift and multiplication coefficient to the incoming light ray.

Considering a point-source, the direct current (DC) gain of the LoS link between a light source and a receiver, which follows a geometric model, can be expressed as [5]

$$H^{(i)} = \frac{A_i(\zeta_i + 1)}{2\pi(d_i)^2} \cos^{\zeta_i}(\phi_i) \cos(\varphi_i) \Psi_i, \tag{1}$$

where A_i and ζ_i are the detector's effective area and the lambertian order, respectively, ϕ_i is the angle of irradiance from the light source to the receiver, φ_i is the angle of incidence of the ray from the light source to the receiver defined as $0 \leq \varphi_i \leq$ field-of-view, and d_i is the distance from the light source to the receiver. Finally, $\Psi_i = f(\varphi_i)g(\varphi_i)$ is the product of gains of the optical filter and non-imaging concentrator. Note that the index i specifies the VLC links, which are light sources (LS)-user, LS-DRIS, and DRIS-user (see Fig. 1).

B. The DRIS Elements and Control

The DRIS is composed of LC-based elements that are characterized by their refractive indices and are sensitive to external fields. Two parameters characterize the emergent signal when a light is reflected on an LC's surface: its power and its direction. It is important to note that these two parameters are influenced by the LC's refractive index. Therefore, a change in the refractive index results in a change in the light power and orientation. It should, however, be noted that the emerged power is calculated based on the impinging light incidence angle.

The DRIS is made of M digital elements [6]. Depending on the power and users' positions, L elements, $L \leq M$, are active at a time. These may or may not be made from the same substance and dye. Depending on the substance and dye used, the DRIS

TABLE I
EXAMPLE OF CONTROL INDICES AND CORRESPONDING v_k, n_k, AND δ_k [9], AND THE EXPECTED ψ_k, FOR $\varphi = 45°$.

Sequence index, k	0	1	2	3	4	5	6	7	8
Phase shift, ψ_k, (^{o})	0	$\frac{\pi}{8}$	$\frac{\pi}{4}$	$\frac{3\pi}{8}$	$\frac{\pi}{2}$	$\frac{5\pi}{8}$	$\frac{3\pi}{4}$	$\frac{7\pi}{8}$	π
$\sin(\psi_k)$	0	0.38	0.71	0.92	1	0.92	0.71	0.38	0
k-th control voltage, v_k (volts)	1.5	1.6	1.8	2	2.2	2.4	2.6	2.8	3
k-th refractive index, n_k	1.74	1.75	1.71	1.67	1.64	-1.61	-1.6	-1.56	-1.55
k-th tilt angle, δ_k, (^{o})	4.50	10.82	21.80	32.0	41.18	49.23	56.16	62.03	66.95
$\frac{\sin(\psi_k)}{n_k}$	0	0.22	0.42	0.55	0.61	0.57	0.45	0.24	0
k-th angle of refraction, θ_k, (^{o})	0	12.6	24.6	33.4	37.7	35	26.7	14.1	0

element may exhibit positive or negative refractive indices, leading to positive or negative reflections [6]. Each element's refractive index (i.e., the birefringence) is tuned independently, resulting in the element being controlled individually. K control sequences, s_k, are simultaneously transferred to the DRIS at a time to this effect.[1] The control of the LC's refractive index and birefringence, Δ_n, which is defined as $\Delta_n = n_o - n_e$, is achieved through the adjustment of the externally applied voltage. The LC's tilt angle, δ, which is the manifestation of birefringence, is therefore controlled by the same voltage and related to both n_o and n_e by [6]

$$\frac{1}{n^2(\delta)} = \frac{\cos^2(\delta)}{n_e^2(\delta)} + \frac{\sin^2(\delta)}{n_o^2(\delta)}. \tag{2}$$

Note that, in the sequel, n means $n(\delta)$. Since the phase shift is a function of the tilt angle [9], (2) also defines the relationship between refractive indices, n_o, n_e, and the phase shift, ψ_k, given between the emerged light and the normal to the LC's surface. The refractive index being dependent on the externally applied voltage, v_k, the tilt angle, phase shift, and transition coefficient, η_k, are also dependent on v_k, where $k \in \{0, 1, 2, \ldots, K\}$ is the element type and $k+1$ is the maximum number of DRIS types, while $L = 2^k$ is the number of active DRIS elements. Each k control sequence is mapped to a control voltage, v_k, to which the LC substance reacts with a refractive index, n_k. The impact of the externally applied voltage on the LC's tilt angle can be modeled as [6]

$$\delta_k = \begin{cases} 0, & V_c > v_k \\ \frac{\pi}{2} - 2\tan^{-1}\left[\exp(V_c - v_k)\right], & v_k > V_c, \end{cases} \tag{3}$$

where V_c is the minimum value of v_c that creates a change in the LC. The DRIS control follows the steps $s_k \Longrightarrow v_k \Longrightarrow f_k(\varphi, n, \psi, \eta)$, where s_k is the k-th control sequence and φ is the light incident angle. Let $s_k \in \{s_0, s_1, \ldots, s_K\}$, $v_k \in \{v_0, v_1, \ldots, v_K\}$, $n_k \in \{n_0, n_1, \ldots, n_K\}$, and $\psi_k \in \{\psi_0, \psi_1, \ldots, \psi_K\}$. The mapping function, $f_k(\varphi, n, \psi, \eta)$, can be given by $f_k(\varphi, n, \psi, \eta) \in \{(\varphi, n_0, \psi_0, \eta_0), (\varphi, n_1, \psi_1, \eta_1), \ldots, (\varphi, n_K, \psi_K, \eta_K)\}$. φ and ψ_k are defined in $[0, \pi]$ and can respectively be expressed as $(\varphi, \psi_k) = (\varphi, \pi k/K)$. The transition coefficient $\eta_k = \eta_o \beta_k$, where η_o and β_k are the initial transition coefficient and a factor depending on the required power at the user, respectively. Examples of ψ_k, n_k, v_k, δ_k, and θ_k values for $k = 0, 1, 2, 3, 4, 5, 6, 7, 8$, corresponding to nine DRIS element types, are provided in Table I.

[1]Note that more than one DRIS element can be controlled with the same code sequence [6], [7], [8].

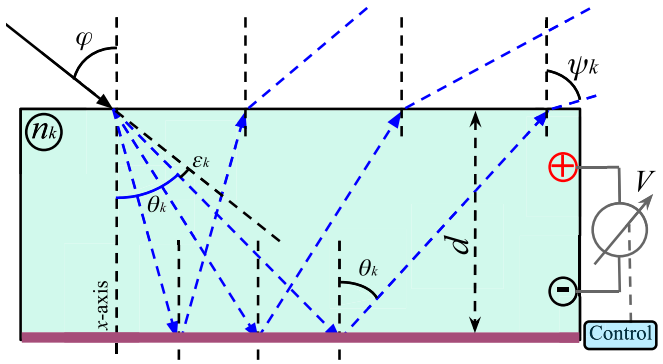

Fig. 2. Impact of externally applied electric field on refractive index and phase shift.

C. Control of the Transition Coefficient, η_k

Considering that light reflection at the bottom of the DRIS unit is lossless, each of the values of η_k are obtained from a double refraction coefficient happening as the impinging signal enters and exits the DRIS structure. Assuming an un-polarized incident light, the transmittance, $T_{i,k}$, as light penetrates into the DRIS structure, is expressed as [10]

$$T_{i,k} = 1 - \frac{1}{2}\left[\frac{\left(\frac{n_k}{n_a}\right)^2\cos(\varphi) - \sqrt{\left(\frac{n_k}{n_a}\right)^2 - \sin^2(\varphi)}}{\left(\frac{n_k}{n_a}\right)^2\cos(\varphi) + \sqrt{\left(\frac{n_k}{n_a}\right)^2 - \sin^2(\varphi)}}\right]^2 - \frac{1}{2}\left[\frac{\cos(\varphi) - \sqrt{\left(\frac{n_k}{n_a}\right)^2 - \sin^2(\varphi)}}{\cos(\varphi) + \sqrt{\left(\frac{n_k}{n_a}\right)^2 - \sin^2(\varphi)}}\right]^2, \tag{4}$$

where n_a is the air refractive index. The two negative terms in (4) are related to the $p-$ and $s-$polarization of the impinging light, respectively [10]. The same Fresnel formula in (4) can be exploited to find the transmittance as the light ray goes out of the DRIS structure, $T_{o,k}$, where n_k/n_a becomes n_a/n_k, and φ is replaced by θ_k. We obtain $T_{i,k} \in \{0.4891, 0.4891, 0.4901, 0.4913, 0.4922, 0.4931, 0.4939, 0.4944, 0.4946\}$ and $T_{o,k} \in \{0.4635, 0.47, 0.4904, 0.4929, 0.3085, 0.4902, 0.4940, 0.4808, 0.4767\}$, leading to the Fresnel reflection coefficient $F_{o,k} \in \{0.2267, 0.2299, 0.2403, 0.2422, 0.1518, 0.2417, 0.2440, 0.2377, 0.2358\}$. The retardation angle, ε_k, shown in Fig. 2, can be approximated as $\varepsilon_k = a + b\delta_k$, $(a, b) \in \mathbb{R}^2$ [9]. Thus, the angle of refraction can be expressed as $\theta_k = \varphi - (a + b\delta_k)$.

Algorithm 1: DRIS Control Process.

Input: n_0, δ_0, η_0, β_k;
procedure Mapping function $f\varphi, n, \psi, \eta$
  Obtain the angle of incidence, φ;
  Define the index, k;
  Obtain the user position;
  Increase v_k;
  while $v_k \geq V_c$ **do**
    $v_k = V_c - \log[\tan(\frac{\pi - 2\delta_k}{4})]$;
  end while
  return ψ_k ((5)) and η_k ((6))
end procedure

Based on Snell's law, the phase shift, ψ_k, can be inferred from

$$\sin\left(\varphi - (a + b\delta_k)\right) = \frac{\sin(\psi_k)}{n_k}, \tag{5}$$

where δ_k is given in (3). Finally, the transition coefficient, η_k, of the light ray through the DRIS is similar to that of a thin film LC structure, and can be expressed as [11]

$$\eta_k = \frac{F_{o,k}\sin^2\left(\frac{4\pi}{2\lambda}n_k x\right)}{1 + F_{o,k}\sin^2\left(\frac{4\pi}{2\lambda}n_k x\right)}, \tag{6}$$

where x is the thickness of the LC's layer and λ is the light wavelength. The proposed DRIS control process is summarized in Algorithm 1. The code sequence is made of three main blocks, including the activation bit, $\{a\} \in \{\{0\}, \{1\}\}$, the phase profile $\{b_1, b_2, \ldots, b_k\}$, and the transition coefficient profile $\{c_1, c_2, \ldots, c_k\}$, leading to a full code sequence structured as $\{a\}\{b_1, b_2, \ldots, b_k\}\{c_1, c_2, \ldots, c_k\}$. Note that this aspect is not studied in this paper.

III. Achievable Rate

The NLoS link contains the diffuse path and the specular reflection link. It is assumed that the diffuse NLoS path has no impact on the system's performance. It is also assumed that the number of users coincides with the number of control sequences, i.e., $U = K$. Thus, the ratio L/K is the number of DRIS elements used to connect a single user, provided that each user is assigned the same number of elements. The total power at the u-th user, $P_{q,u}$, is the sum of power components transiting through the LoS and NLoS-DRIS links, and is given by

$$P_{q,u} = \rho_u \left[H_{q,u}^{(1)} + \underbrace{H_h \eta_k H_g}_{H_{q,u}^{(2)}} \right] P_q, \tag{7}$$

where ρ_u and P_q are the receiver's responsiveness and optical power of the q-th LS, respectively. H_h and H_g are the DC gains of the LS-DRIS and DRIS-user links, respectively. $H_{q,u}^{(j)}$ is the j-th link from the q LS to the u-th user, $j \in \{\text{LoS, NLoS}\}$. Similarly, the received temporal signal, $y_{q,u}(t)$, is the sum of lights from the LoS and NLoS-DRIS links, and is given by

$$y_{q,u}(t) = y_{q,u}^{(1)}(t) + y_{q,u}^{(2)}(t) + n_u(t), \tag{8}$$

where $n_u(t)$ is the additive white Gaussian noise with zero mean and variance σ^2 defined by $n_u \sim \mathcal{N}(0, \sigma^2)$. For the transmitted vector $\boldsymbol{x} = [x_1, x_2, \ldots, x_Q]^T$, the LoS signal from the q-th LS at the u-th user can be expressed as

$$y_{q,u}^{(1)}(t) = \rho_u \left[H_{q,u}^{(1)} P_q x_q(t) + \sum_{i=1, i\neq q}^{Q} H_{i,u}^{(1)} P_i x_i(t) \right], \tag{9}$$

while the DRIS-based NLoS component can be expressed as

$$y_{q,u}^{(2)}(t) = \rho_u \left[H_{q,u}^{(2)} P_q x_q(t) + \sum_{i=1, i\neq q}^{Q} H_{i,u}^{(2)} P_i x_i(t) \right]. \tag{10}$$

The transmitted signal, $x_q, q \in \{1, 2, \ldots, Q\}$, is bounded by 0 and ∂, where ∂ is the peak-input intensity, and the sum of individual powers, $\sum_{i=1}^{Q} P_i$, is upper bounded by p_q [12], [13]. These two constraints regulate transmission in indoor VLC systems. The fact that illumination is calculated to satisfy the environment usage places an upper limit on the optical power [12], [13]. Hence, $p_q/\partial < Q/2$, is a fair combination between the total power, p_q, and the peak-input intensity, ∂, and yields an upper bound to the point-source channel capacity of a VLC system as [12], [13]

$$C_{q,u} = \frac{1}{2} B \log_2 \left[1 + \frac{\exp(1)}{2\pi} \gamma_{q,u}^2 \right], \tag{11}$$

where B is the transmission bandwidth, $\exp(1)$ is the base of the natural logarithm, and $\gamma_{q,u}$ is the signal-to-noise ratio at the u-th user, which is given by

$$\gamma_{q,u} = \frac{\rho_u^2 \left\{ H_{q,u}^{(1)} + \frac{K}{L} H_{q,u}^{(2)} \right\}^2 P_q^2}{N_{q,u}^0}, \tag{12}$$

where K/L is the portion of DRIS elements serving the u-th user and the noise PSD, $N_{u,q}^0$, can be expressed as

$$N_{q,u}^0 = \sigma_u^2 + \rho_u^2 \sum_{i=1, i\neq q}^{Q} \left\{ \left(H_{i,u}^{(1)} + \frac{K}{L} H_{i,u}^{(2)} \right) P_i \right\}^2. \tag{13}$$

Therefore, the system's achievable transmission rate can be expressed as

$$R_a = \sum_{u=1}^{U} \frac{1}{2} B \log_2 \left[1 + \frac{\exp(1)}{2\pi} \frac{\rho_u^2 \left\{ H_{q,u}^{(1)} + \frac{K}{L} H_{q,u}^{(2)} \right\}^2 P_q^2}{N_{q,u}^0} \right]. \tag{14}$$

In case of total obstruction of the LoS link, the achievable transmission rate in (14) reduces to

$$R_a^{(2)} = \sum_{u=1}^{U} \frac{1}{2} B \log_2 \left[1 + \frac{\exp(1)}{2\pi} \frac{\rho_u^2 \left\{ \frac{K}{L} H_{q,u}^{(2)} \right\}^2 P_q^2}{N_{q,u}^{0(2)}} \right], \tag{15}$$

and represent the achievable rate due to the NLoS path through the DRIS alone. In (15), $N_{u,q}^{0(2)} = \sigma_u^2 + \rho_u^2 \sum_{i=1, i\neq q}^{Q} \{\frac{K}{L} H_{i,u}^{(2)} P_i\}^2$.

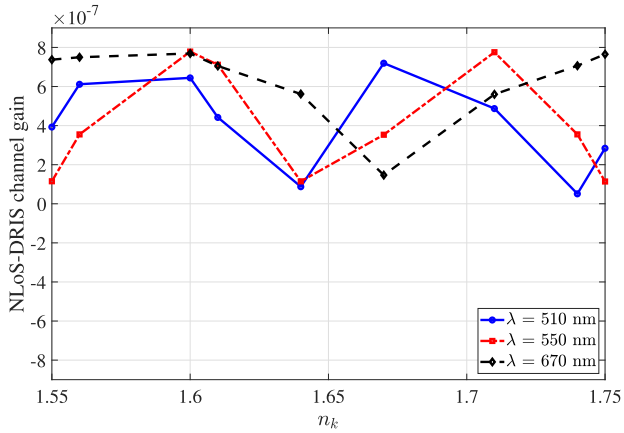

Fig. 3. NLoS-DRIS channel DC gain vs. n_k.

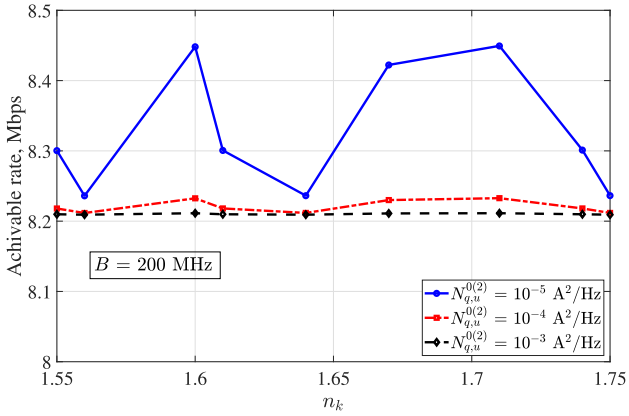

Fig. 4. Achievable transmission rate of the NLoS link vs. refractive index n_k for specific values of the noise PSD.

IV. Numerical Results

Consider a DRIS-assisted indoor VLC system where the LoS link is totally obstructed. The deployment of the RIS introduces two sub-channels h and g as shown in Fig. 1. The first sub-channel is characterized by $d_h = 2$ m, the active area of the DRIS element is $A_r = w_1 \times w_2 = 2.5 \times 10^{-4}$ m^2, an incident angle of $\varphi_h = 45°$, an angle of irradiance $\phi_h = 45°$, the filter function, $\Psi_h = 1$, and a lambertian order, $\zeta_q = 1$. It is assumed that the receiver is equipped with an adjustable receiving system to considerably reduce the probability of reflected signal obstruction, i.e., the PD orientation is adjusted to align with the impinging light. The DRIS active area is small enough such that light reflection on it is considered as a point source. For the purpose of comparison, we consider nine users, all located at a distance $d_g = 2$ m from the DRIS structure. However, each user is oriented in such a way to be linked by emerged lights with phase shift 0, $\frac{\pi}{8}$, $\frac{\pi}{4}$, $\frac{3\pi}{8}$, $\frac{\pi}{2}$, $\frac{5\pi}{8}$, $\frac{3\pi}{4}$, $\frac{7\pi}{8}$, and π, see Table I-row 2. It is also considered that the filter functions at the users is $\Psi_g = 1$. The users are arranged such that the incidence angles, $\phi_g = 0°$, and the light is distributed at the DRIS with a lambertian order $\zeta_g = 1$. The users are equipped with a photodetector of active effective area, $A_u = 10^{-3}$ m^2. We consider a 10 W transmitter, a transmission bandwidth of 200 MHz, three different wavelengths, 510 nm, 550 nm, and 670 nm, and the LC parameters used are listed in Table I. The transition coefficient given in Table I is used to find the emerged light power in the corresponding direction.

Figs. 3, 4, and 5 depict the impact of the LC's intrinsic parameters on the DC channel gain and achievable rate. The non-linear aspect of the LCs is demonstrated in the results presented in these figures. This is clearly shown in Figs. 3 and 4, where the DC gain and the achievable rate are provided considering the refractive index, wavelength, and noise PSD. $|n_k|$ is used in these two figures in accordance with the fact that the channel gain, $H^{(2)}_{q,u}$, and the achievable rate, $R^{(2)}_a$, are positive for any values of the refractive index. Fig. 3 also shows the non-linearity of the DC channel gain with respect to both the refractive index and wavelength. This can be observed on the DC channel gain that fluctuates between 10^{-7} and 7.5 $\times 10^{-7}$ for $|n_k| \in [1.6, 1.67]$.

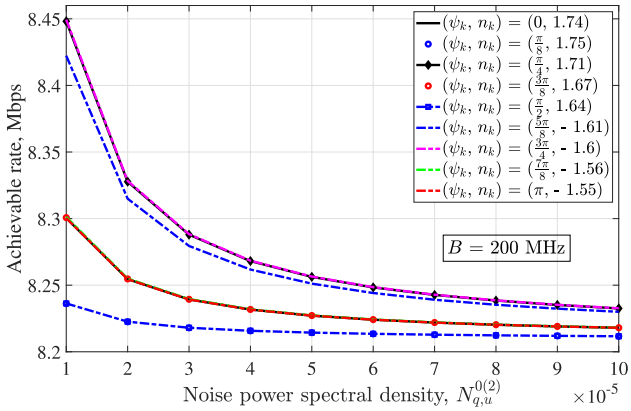

Fig. 5. Achievable transmission rate of the NLoS link vs. noise PSD.

These are 6.444 $\times 10^{-7}$, 8.758 $\times 10^{-8}$, and 7.196 $\times 10^{-7}$ for $\lambda = 510$ nm, 7.689 $\times 10^{-7}$, 1.147 $\times 10^{-7}$, and 3.532 $\times 10^{-7}$ for $\lambda = 550$ nm, 7.689 $\times 10^{-7}$, 5.616 $\times 10^{-7}$, and 1.467 $\times 10^{-8}$ for $\lambda = 670$ nm, respectively. This non-linearity can also be noticed in Fig. 4 where, for $\lambda = 550$ nm, the achievable rate presents a saw-tooth curve. For the same 10^{-4} A^2/Hz noise PSD, the achievable rates are respectively 8.448, Mbps, 8.236 Mbps, and 8.422 Mbps for $n_k = 1.6$, 1.64, and 1.67. For 10^{-5} A^2/Hz noise PSD, and considering the same values of n_k, 8.235 Mbps, 8.209 Mbps, and 8.211 Mbps can be achieved, respectively. For a noise PSD in the range of 10^{-5} to 10^{-4}, up to 217.50 kbps of transmission rate variation can be observed. On the contrary, Fig. 4 depicts an almost constant achievable rate of 8.211 Mbps for $n_k = 1.6$, 1.64, and 1.67. This means that the achievable rate tends to its lower limit as the noise PSD approximates 10^{-3} A^2/Hz for the considered system using a light with wavelength $\lambda = 550$ nm. Furthermore, Fig. 5 depicts the achievable rate in terms of the noise PSD for a set of refractive index values, $n_k \in \{-1.61\ -1.6\ -1.56\ -1.55\ 1.64\ 1.67\ 1.71\ 1.74\ 1.75\}$. In light of the results shown in this figure, it should be noted that symmetric values of refractive indices do not lead to the same achievable rate. The reason is that each value of n_k corresponds to a different transition coefficient and phase shift, for an angle of

incidence. There is no linear relationship between the refractive index, transition coefficient, and phase shift.

V. Implementation Complexity and Conclusion

The refractive index of the DRIS element is determined by the user's position. Therefore, the DRIS control steps are as follows: (i) The user communicates its position to the DRIS. (ii) Based on this, the necessary direction is calculated. (iii) The control voltage is then adjusted to obtain an updated light orientation, leading to the user's connection. In practice, the implementation of this control is not complex and has been well investigated in the literature [14], [15].

In this paper, LC-based DRIS-assisted indoor VLC systems are studied. The impacts of the DRIS's intrinsic parameters on the achievable rate are investigated. The DRIS control process based on externally applied voltages is analyzed. The corresponding values of the tilt angle, angle of refraction, refractive index, transition coefficient, and phase shift are evaluated. These values are used to assess the received power and achievable rate for a selected set of discrete phase shifts. This assessment was made considering several values of noise PSD and light wavelength. It is observed that the control of LC-based DRIS elements, obtained emerged power, and achievable transmission rate are not linear functions of the LC parameters, and up to 217.50 kbps of transmission rate variation can be observed.

References

[1] H. Abumarshoud et al., "LiFi through reconfigurable intelligent surfaces: A new frontier for 6G?," *IEEE Veh. Technol. Mag.*, vol. 17, no. 1, pp. 37–46, Mar. 2022.

[2] Y. Liu et al., "Reconfigurable intelligent surfaces: Principles and opportunities," *IEEE Commun. Surveys Tuts.*, vol. 23, no. 3, pp. 1546–1577, Jul.–Sep. 2021.

[3] S. Aboagye, A. R. Ndjiongue, T. M. N. Ngatched, O. A. Dobre, and H. V. Poor, "RIS-assisted visible light communication systems: A tutorial," *IEEE Commun. Surv. Tut.*, early access, Dec. 2022.

[4] C. Yihan et al., "Joint deployment and resource management for VLC-enabled RISs-assisted UAV networks," *IEEE Trans. Wireless Commun.*, early access, Apr. 2022.

[5] S. Aboagye et al., "Intelligent reflecting surface-aided indoor visible light communication systems," *IEEE Commun. Lett.*, vol. 25, no. 12, pp. 3913–3917, Dec. 2021.

[6] A. R. Ndjiongue et al., "Digital RIS (DRIS): The future of digital beam management in RIS-assisted OWC systems," *IEEE/OSA J. Lightw. Technol.*, vol. 40, no. 16, pp. 5597–5604, Aug. 2022.

[7] L. Zhang et al., "Space-time-coding digital metasurfaces," *Nature Commun.*, vol. 9, no. 1, pp. 1–11, Oct. 2018.

[8] T. J. Cui et al., "Coding metamaterials, digital metamaterials and programmable metamaterials," *Nat. Sci. Appl.*, vol. 3, no. 10, pp. 1–9, Oct. 2014.

[9] V. Belyaev et al., "Phase retardation vs. pretilt angle in liquid crystal cells with homogeneous and inhomogeneous LC director configuration," *Opt. Exp.*, vol. 21, no. 4, pp. 4244–4249, Feb. 2013.

[10] M. Hebert, "Reflection and transmission of light by a flat interface, Fresnel's formulae," Institut d'Opt., pp. 1–11, Jan. 2013.

[11] P. Poole et al., "Experiment and simulation of novel liquid crystal plasma mirrors for high contrast, intense laser pulses," *Sci. Rep.*, vol. 6, no. 1, pp. 1–8, Aug. 2016.

[12] A. Chaaban et al., "Capacity bounds and high-SNR capacity of MIMO intensity-modulation optical channels," *IEEE Trans. Wireless Commun.*, vol. 17, no. 5, pp. 3003–3017, May 2018.

[13] A. R. Ndjiongue et al., "On the capacity of RIS-assisted intensity-modulation optical channels," *IEEE Commun. Lett.*, vol. 26, no. 2, pp. 389–393, Feb. 2022.

[14] J. Lin et al., "Manipulation of random lasing action from dye-doped liquid crystals infilling two-dimensional confinement single core capillary," *IEEE Photon. J.*, vol. 7, no. 3, pp. 1–9, Jun. 2015.

[15] C. G. L. Khoo et al., "Effect of copper lamination on the rheological and copper adhesion properties of a thermotropic liquid crystalline polymer used in PCB applications," *IEEE Trans. Compon. Packag. Technol: Part C*, vol. 20, no. 3, pp. 219–226, Jul. 1997.